Journal of Power Sources 234 (2013) 147–153

Contents lists available at SciVerse ScienceDirect

Journal of Power Sources

journal homepage: www.elsevier.com/locate/jpowsour

Particle size dependence of polarization of Ni/YSZ cermet anodes for solid oxide fuel cells

Tsuyoshi Kawashima [a,*], Shogo Miyoshi [b], Yasushi Shibuta [b], Shu Yamaguchi [b]

[a] Training Institute of Pipeline Engineering, Tokyo Gas Co., Ltd., Suehiro-cho 1-7-7, Tsurumi-ku, Yokohama 230-0045, Japan
[b] Department of Materials Engineering, School of Engineering, The University of Tokyo, Hongo 7-3-1, Bunkyo-ku, Tokyo 113-8656, Japan

HIGHLIGHTS

- We examine the triple-phase boundary(TPB) of Ni/YSZ cermet by computer simulation.
- The length is a concave function of the Ni-volume fraction with a maximal value.
- The maximal TPB length reduces with increasing the particle size of Ni or that of YSZ.
- We derive a steady-state current–potential curve as a function of particle sizes.

ARTICLE INFO

Article history:
Received 10 September 2012
Received in revised form
28 December 2012
Accepted 19 January 2013
Available online 28 January 2013

Keywords:
Solid oxide fuel cell
Anode
Particle size
Monte Carlo simulation
Polarization
Triple-phase boundary

ABSTRACT

A Monte Carlo simulation and the steady-state anodic polarization measurement have been performed to examine the particle size dependence of the polarization of nickel yttria-stabilized zirconia (Ni/YSZ) cermet anodes for solid oxide fuel cells. The triple-phase boundary (TPB) length in the model system is estimated by a Monte Carlo simulation using a simple cubic lattice model. The estimated TPB length is concave with respect to the nickel-volume fraction X for all particle-size combinations, and the maximal TPB length decreases as the size of the nickel or that of YSZ increases. The current–potential curve of the electrode reaction of the cermet anode has been estimated as a function of the sizes of the nickel particles and the YSZ particles on the basis of the calculated TPB length and the experimental data at $X = 0.44$ and at 1273 K. In the design of the SOFC anode, the estimated relation between polarization and particle size can be practically applicable to the range in which secondary particles do not form.

1. Introduction

Solid oxide fuel cells (SOFCs) have been widely developed for many years, and various materials have been examined as candidates for the anode material. In an earlier stage, graphite [1] has been used as an anode material, although it is ultimately not useful in practical sense due to an active enrollment in the electrode reaction observed as corrosion. Subsequently, platinum and several transition metals such as iron, cobalt and nickel have been examined [2]. However, these metals also do not satisfy the practical needs of SOFCs due to the corrosion in case of iron or the delamination after sintering in case of iron and nickel, in addition to the cost problem with platinum and cobalt [3]. Such corrosion and sintering/delamination are mainly caused when single phases of transition metals are used as anode. Spacil [4] has overcome such problems by using nickel ytteria-stabilized zirconia (Ni/YSZ) cermet as anode. Since then, this cermet composite has become a standard anode material. In practice, the electrochemical properties of the cermet used as SOFC anodes strongly depend on the composition and morphology. Therefore, numerous studies have been performed to optimize these factors, focusing on the composition [5–7], the size of the starting powders [6,8], and the sintering temperature [9,10], and so on. However, the optimum fabrication process for the Ni/YSZ cermet has not been yet established despite of the numerous efforts described above.

Through much effort to find the optimum condition for the Ni/YSZ cermet fabrication, some of the key factors to understand the fundamental mechanisms for the electrode reaction have been proposed. For example, the DC and AC polarization studies of Ni-patterned anodes [11–14] suggest that the electrode-reaction

* Corresponding author. Tel.: +81 45 505 7305; fax: +81 45 500 2013.
E-mail address: tsuyoshi@tokyo-gas.co.jp (T. Kawashima).

0378-7753/$ – see front matter © 2013 Elsevier B.V. All rights reserved.
http://dx.doi.org/10.1016/j.jpowsour.2013.01.125

occurs mainly at the triple-phase boundary (TPB) composed of nickel, YSZ and gas phases. Therefore, the TPB length per unit volume is a predominant factor determining the anode performance. In addition, the cermet microstructure has been studied widely using various techniques [15–18]. For example, Wilson and coworkers [15] have estimated the TPB length of their anode on the basis of a three-dimensional reconstruction technique involving focused ion beam scanning electron microscopy (FIB-SEM). Shikazono et al. [17] investigated the correlation between the microstructure and electrochemical properties of the anode in addition to the estimation of the TPB length. In contrast, we have previously investigated the effect of the particle size of the starting powders on the electrochemical properties of the Ni/YSZ cermet anode experimentally [19] and reported that the DC anodic polarization strongly depends on the particle size, although we have never been able to quantitatively elucidate the correlation factors. In this study, after summarizing the experimental results for the steady-state anodic polarization curves, a Monte Carlo simulation with a simple cubic lattice model is performed to examine the anodic polarization as a function of the size of nickel and YSZ particles, focusing on the TPB length. Then, we derive an analytical model for the polarization of the Ni/YSZ cermet anode as a function of the size of nickel and YSZ particles, which should be useful for estimating the polarization as a function of particle size of the starting powders in the design of a practical SOFC anode.

2. Experimental

2.1. Electrochemical measurements

Ni/YSZ cermet anodes are fabricated as follows. Spherical nickel or nickel oxide powders and YSZ (ZrO_2-8 mol% Y_2O_3) powders, which are weighted so that the nickel-volume fraction is 0.44 of the total solids, are mixed in a rocking mixer and suspended in 2-propanol to produce anode slurries. By the combination of six different sizes of nickel or nickel oxide powders (mean diameter: 0.20–200 μm, standard deviation: 15–38% of the mean diameter) and seven sizes of YSZ powders (mean diameter: 0.11–3.5 μm, standard deviation: 13–41% of the mean diameter) are mixed to prepare 18 matrix samples. The slurry is painted on one face of a YSZ electrolyte disk (ZrO_2-8 mol% Y_2O_3, 20 mm in diameter and 2 mm in thickness) and fired at 1723 K in air for 43.2 ks. Resultant anode thickness, geometrical area and porosity are approximately 100 or 200 μm, 2.83×10^{-5} m^2 (6 mm in diameter) and 0.31 to 0.45, respectively. Pt paste is painted on another face of the disk as the counter electrode (6 mm in diameter) and Pt wire (0.5 mm in diameter) is wound around the side of the disk as the reference electrode.

The steady-state DC polarization measurements are made at 1273 K using the following electrochemical cell: H_2/N_2, Ni/YSZ cermet |YSZ| Pt, air. The H_2/N_2 gas mixture (oxygen-partial pressure: 1×10^{-14} Pa) and air are fed to the anode (working electrode) and the counter electrode, respectively and the reference electrode is exposed to air. The current between the working electrode and the counter electrode is controlled by a galvanostat (Toho-Giken, Potentiostat/Galvanostat 2000), and the steady-state potential is measured. The ohmic loss is subtracted from the measured potential using a current interruption technique (Toho-Giken, CI-01).

2.2. Experimental results

Typical steady-state anodic polarization curves of Ni/YSZ cermet anodes composed of YSZ particles with a constant size without ohmic losses are shown in Fig. 1. The curves are considerably different by the nickel-particle size, and show lower overpotential on smaller nickel particles. Because they do not exhibit a linear region, electrochemical parameters cannot be determined by so-called Tafel extrapolation method.

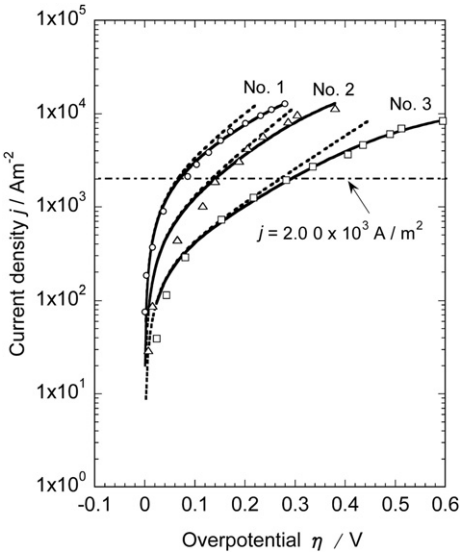

Fig. 1. Steady-state anodic polarization curves of three different Ni/YSZ cermet anodes at 1273 K and $p_{O_2} = 1 \times 10^{-14}$ Pa for samples No. 1 (0.51, 0.35), No. 2 (74, 0.35) and No. 3 (200, 0.35) where the numbers in the brackets are d_{Ni} and d_{YSZ} (μm), respectively. Symbols represent experimental values and solid lines represent the regression curves of Eq. (1) obtained by the Levenberg–Marquardt method. Dashed lines represent the estimated activation polarizations calculated from Eq. (1) by using the electrochemical parameters listed in Table 1, assuming $|j_{a,l}| >> |j_0|$ and $|j_{c,l}| >> |j_0|$.

The steady-state polarization curve, whose expression is derived in Appendix A, is written as follows,

$$j = \frac{j_0\left\{\exp\left(\frac{\alpha_a zF\eta}{RT}\right) - \exp\left(-\frac{\alpha_c zF\eta}{RT}\right)\right\}}{1 + \frac{j_0}{j_{a,l}}\exp\left(\frac{\alpha_a zF\eta}{RT}\right) + \frac{j_0}{j_{c,l}}\exp\left(-\frac{\alpha_c zF\eta}{RT}\right)}, \quad (1)$$

where j is the current density (A m^{-2}), j_0 is the exchange current density (A m^{-2}), j_l is the limiting current density (A m^{-2}), α is the transfer coefficient, z is the number of electrons involved in the electrode reaction, F is Faraday's constant (96487 C mol^{-1}), η is the overpotential (V), R is the gas constant (8.314 J mol^{-1} K) and T is the absolute temperature (K). In addition, subscripts a and c represent anodic and cathodic side, respectively. Using the Levenberg–Marquardt method [20] for the non-linear least squares minimization, one may find that the electrochemical parameters, such as j_0, $\alpha_a z$, $\alpha_c z$, $j_{a,l}$ and $j_{c,l}$ in Eq. (1) at 1273 K are determined by curve-fitting to the experimental results for the anodes with combinations of the nickel particle size d_{Ni} (μm) and the YSZ particle size d_{YSZ} (μm) noted as (d_{Ni}, d_{YSZ}): (0.51, 0.35), (74, 0.35) and (200, 0.35). Fig. 1 also shows the fitting curves describing the steady-state anodic polarization curve. The parameters determined by fitting are listed in Table 1. The sum of $\alpha_a z_a$ and $\alpha_c z_c$ becomes nearly two for all cases. Note that the limiting current densities are one or two orders of magnitude larger than the exchange current density. Upon

Table 1
Electrode-reaction parameters of H_2/N_2, Ni/YSZ cermet | YSZ electrolyte at 1273 K obtained from the measurement of the steady-state anodic polarization curve.

No.	d_{Ni} (μm)	d_{YSZ} (μm)	j_0 (A m^{-2})	$\alpha_a z$	$\alpha_c z$	$j_{a,l}$ (A m^{-2})	$j_{c,l}$ (A m^{-2})
1	0.51	0.35	1.53×10^3	1.04	0.94	3.12×10^4	-3.03×10^4
2	74	0.35	5.67×10^2	1.11	0.81	2.50×10^4	-2.31×10^4
3	200	0.35	2.19×10^2	0.89	1.15	1.22×10^4	-1.92×10^4

assumption that $|j_{a,l}| >> |j_0|$ and $|j_{c,l}| >> |j_0|$ in Eq. (1), the calculated steady-state current–potential curves are also displayed as dashed lines. The differences between these two types of curves for each particle size represent the concentration overpotentials, which originate in the vicinity of the reactive site near the TPBs [21].

3. Monte Carlo simulation

3.1. A simple cubic lattice model

The Ni/YSZ cermet is modeled by a simple cubic lattice consisting of 64 × 64 × 64 unit cubes. Each unit cube corresponds to either nickel or YSZ phase, as shown in Fig. 2. The size of nickel and YSZ sites is defined by an aggregate of the unit cube. That is, an aggregate of n^3 nickel (or YSZ) unit cubes represents a nickel (or YSZ) site with the size of d_{Ni} (or d_{YSZ}) = n. These aggregates representing nickel and YSZ sites are randomly located in the cubic lattice, which is sandwiched between the YSZ electrolyte substrate and the current corrector. The actual Ni/YSZ cermet consists of three phases, that is, nickel, YSZ and a gas phase. In the model, each unit cubic is occupied by either nickel or YSZ phase. The gas phase is then regarded to be located at edges that are shared by four adjacent unit cubes. Fig. 3(a-1) and (a-2) shows examples of the cross section of an edge shared by four adjacent unit cubes. We focus on a unit cube in the four adjacent unit cubes occupied by Ni or YSZ phase. If both of the two nearest neighbor cubes are occupied by the other phase, two TPBs are considered to be formed in the vicinity of the common edge. Therefore, four TPBs exist in the vicinity of one common edge (Fig. 3(a-1)) and two TPBs exist at the common edge (Fig. 3(a-2)). Fig. 3(b) presents the sum of TPBs in the vicinity of the common edge in all combinations of sixteen patterns of four adjacent unit cubes.

3.2. Calculation procedure

The TPB length in the model system is determined using a Monte Carlo simulation as follows. The configuration of each unit cube in the system as nickel or YSZ is picked using a uniform random number between zero and one. Enough random numbers are generated to cover the number of sites. When the random number generated is smaller than a threshold number (between zero and one), the corresponding site is regarded as being occupied by a nickel phase and vice versa. Here, X is defined as the number of unit cubes occupied by a nickel phase divided by 64^3. Therefore, X is equivalent to the nickel-volume fraction in the model system. A group of connecting nickel sites is defined as a nickel cluster, and so is the same for YSZ sites. The nickel site belonging to the cluster that

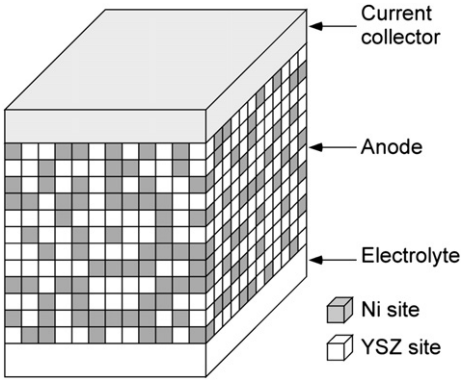

Fig. 2. A schematic illustration of a simple cubic lattice model for the Ni/YSZ cermet sandwiched between the YSZ electrolyte substrate and the current collector. Gray and white cubes represent nickel and YSZ sites, respectively.

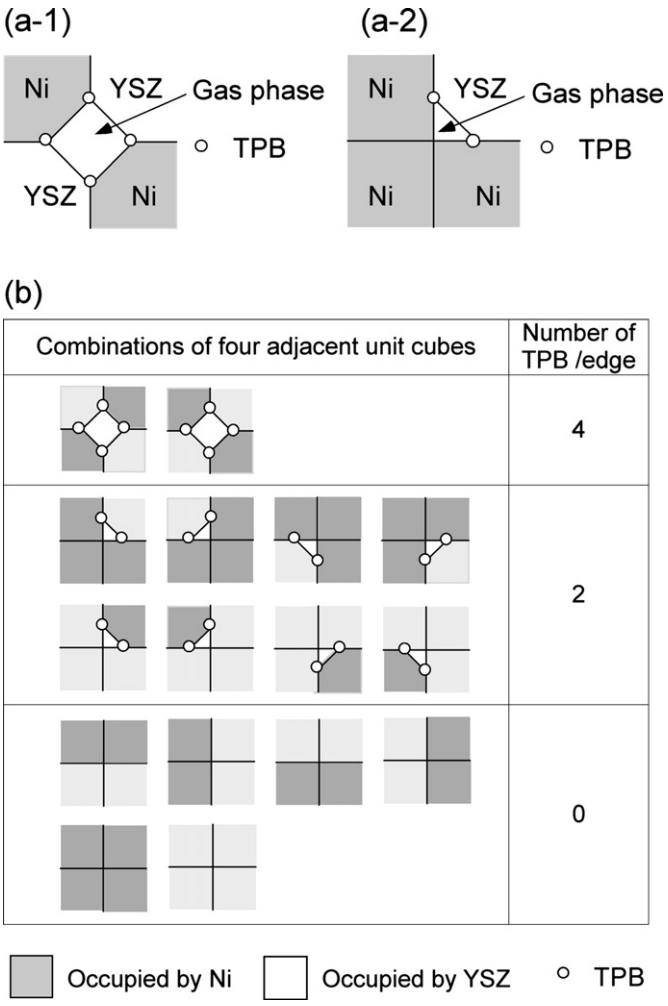

Fig. 3. (a-1) and (a-2) Definition of the triple-phase boundary(TPB) illustrated in the cross sections of four adjacent unit cubes in the simple cubic lattice model. (b) Combinations of four adjacent unit cubes and the number of TPB corresponding to each combination.

is in contact with the current collector is called a percolating site. In the same way, the YSZ site belonging to the cluster contacting the YSZ electrolyte is regarded as a percolating site. This approach assumes that only percolating nickel and YSZ sites participate in an electrode reaction because reaction proceeds when electrons transferred from the current corrector through the nickel phase and oxygen vacancies transferred from the electrolyte through the YSZ phase meet at TPB.

The Hoshen–Kopelman algorithm [22] is employed to define the percolating site in the model system. When a TPB is formed by four adjacent unit cubes in percolating sites, it is regarded as an effective TPB, and the sum of the effective TPB length, l_{TPB}, is calculated under the assumption that the length of the TPB/edge is 0.5 unit lengths. The nickel-volume fraction X is set to cover the range from 0.180–0.352 to 0.620–0.793 with an incremental step of 0.001–0.005. We examined various site–size combinations of d_{Ni} and d_{YSZ}, notated as (d_{Ni}, d_{YSZ}) of (1, 1), (2, 1), (4, 1), (6, 1), (8, 1), (1, 2), (1, 4), (1, 6) and (1, 8), and each X, d_{Ni} and d_{YSZ}, and l_{TPB} is estimated from the average of ten calculations for each case.

3.3. Calculation results

Fig. 4 shows the calculated l_{TPB} as a function of X for seven combinations of d_{Ni} and d_{YSZ}. The estimated standard mean errors

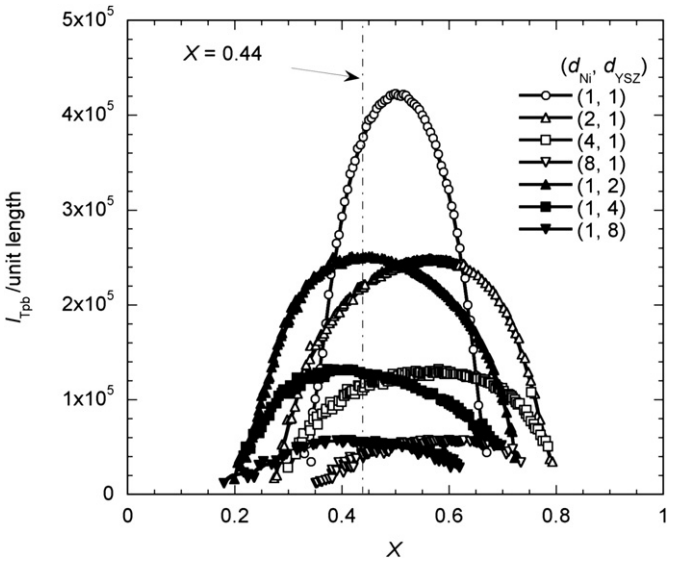

Fig. 4. l_{TPB} as a function of the nickel-volume fraction X with various sizes of nickel (d_{Ni}) and YSZ sites (d_{YSZ}) obtained from the Monte Carlo simulation. The unit length represents a length of the unit cube edge.

with 95% confidence at $X = 0.44$ from ten calculations are 0.29, 0.37, 0.98, and 2.4% for the site–size combinations (1, 1), (2, 1), (4, 1) and (8, 1), respectively. In general, l_{TPB} is a concave function of X with a maximal value for all site–size combinations. The l_{TPB} for (1, 1) reaches a maximum at $X = 0.50$, which corresponds to 54% of the total length of edges in $64 \times 64 \times 64$ unit cubes. The maximal value of the l_{TPB} decreases with increasing either d_{Ni} in (d_{Ni}, 1) or d_{YSZ} in (1, d_{YSZ}). Moreover, the X value that gives the maximal l_{TPB} becomes larger, but always smaller than 0.50 when $d_{Ni} > 1$ and $d_{YSZ} > 1$, respectively.

Table 2 shows l_{TPB} in a unit volume, vl_{TPB} (m m^{-3}), in comparison with vl_{TPB} estimated by a three-dimensional reconstruction technique using FIB-SEM [15,16] and vl_{TPB} calculated by a spherical model [23]. The calculated data are converted to vl_{TPB} by the equation $vl_{TPB} = l_{TPB}/64^3$, assuming that the edge length of the unit cube is 1 μm. Interestingly, the calculated values of vl_{TPB} are on the order of 10^{12}, which agrees with the estimated values from both FIB-SEM experiments and the spherical model. In particular, it is confirmed that the results in this study are in good agreement with the results from the spherical model with respect to following four points; vl_{TPB} takes the maximum (i) at $X = 0.50$ when $d_{Ni} = d_{YSZ}$, (ii) at $X > 0.50$ when $d_{Ni} > d_{YSZ}$, (iii) at $X < 0.50$ when $d_{Ni} < d_{YSZ}$, and (iv) the value of vl_{TPB} for (1, n) at $X = 0.50$ equals that for (n, 1).

Fig. 5 shows the TPB lengths for $X = 0.44$, 0.50 and 0.54 as functions of d_{Ni} and d_{YSZ} in case of site–size combinations of (d_{Ni}, 1) and (1, d_{YSZ}). d_{Ni} and d_{YSZ} smaller than one unit length are the normalized lengths: for example, $d_{Ni} = 0.25$ in Fig. 5 represents the effective length, which is equal to the TPB length of (1, 4) multiplied by $1/4 \times 4^3$. The relationship between l_{TPB} and the site sizes can be regressed to a power function for each composition in the range considered, and the data are fitted to the following function,

$$l_{TPB} = A \times d^n \quad (, \text{ or } \log l_{TPB} = \log A + n \log d), \tag{2}$$

where d and n are the site size of Ni or YSZ and the slope of the fitted line, respectively, and log A is the intercept at log $d = 0$. The coefficient A and the exponent n represent the effect of the composition and that of the site size to l_{TPB}, respectively. The fitted lines are shown in Fig. 5 and parameters A and n obtained by the fitting are summarized in Table 3. l_{TPB} is proportional to the power of approximately minus one of d_{Ni} and d_{YSZ}. This value is explained by the following geometrical relation. The surrounding length of one side of a cubic with the edge length of d_0 is $4d_0$. When the cubic is divided into $(d_0/d)^3$ cubes with an edge length of d, the one side is divided into $(d_0/d)^2$ squares. The sum of the surrounding lengths of the sides of $(d_0/d)^2$ squares is $4d_0^2/d$, which is d_0/d times the length of the initial side. Therefore, the possible TPB length becomes inversely proportional to the site size. Actually, l_{TPB} for $X = 0.44$ with respect to d_{Ni} and d_{YSZ} can be approximated as follows, because the coefficients A for the case of d_{Ni} and d_{YSZ} are the same value.

$$l_{TPB} \approx \frac{4.32 \times 10^5}{d_{Ni} d_{YSZ}}. \tag{3}$$

4. Discussion

We discuss the anodic polarization as a function of site sizes on the basis of the experimental and calculation results. In particular, an equation for the polarization of the Ni/YSZ cermet anode as a function of d_{Ni} and d_{YSZ} will be derived. Here, current densities j_0, $j_{a,l}$ and $j_{c,l}$ are assumed to be proportional to the TPB length per unit area, al_{TPB} (m m^{-2}),

$$j_0 = k_1\, al_{TPB}, \quad j_{a,l} = k_2\, al_{TPB} \quad \text{and} \quad j_{c,l} = k_3\, al_{TPB}, \tag{4}$$

where k_1, k_2 and k_3 are proportionality constants with dimension of A m^{-1}. In general, it is considered that the thickness of anodic reaction area is approximately within 10 μm or less from the anode/electrolyte interface [24]. Therefore, the effect of the anode thickness on al_{TPB} is not taken into account in this study, because the anode thickness under discussion is of 100 μm or greater. For the Ni/YSZ cermet with a thickness of more than 10 μm, al_{TPB} is expressed from Eq. (3) as follows:

$$al_{TPB} = \frac{k_4}{d_{Ni} d_{YSZ}}, \tag{5}$$

where k_4 (m m^{-2} μm^2) is a proportionality constant assumed to be constant here for simplicity, whereas it may actually strictly depend

Table 2
The length of the triple-phase boundary per volume, vl_{TPB}, from Monte Carlo simulation. Values from the literature based on experiments using FIB-SEM [15,16] and calculation by the spherical model [23] are also listed for comparison. X and P represent the nickel-volume fraction of the total solids and the porosity in percentage, respectively.

Source	Particle size (μm)		Volume fraction		vl_{TPB} (m m^{-3})	Method
	d_{Ni}	d_{YSZ}	X	P		
This study	1.0	0.5	0.322	–	1.75×10^{12}	Simple-cubic lattice model
This study	1.0	1.0	0.50	–	1.61×10^{12}	Simple-cubic lattice model
This study	2.0	2.0	0.50	–	4.03×10^{11}	Simple-cubic lattice model
Wilson et al. [15]	1.0[a]	0.5[a]	0.322	0.195	2.70×10^{12}	FIB-SEM
Iwai et al. [16]	1.0[a]	1.0[a]	0.50	0.50	$1.067–1.659 \times 10^{12}$	FIB-SEM
Janardhanan et al. [23]	2.0	2.0	0.50	0.30	3.3×10^{12}	Spherical model

[a] These values are estimated from reconstruction images in their papers.

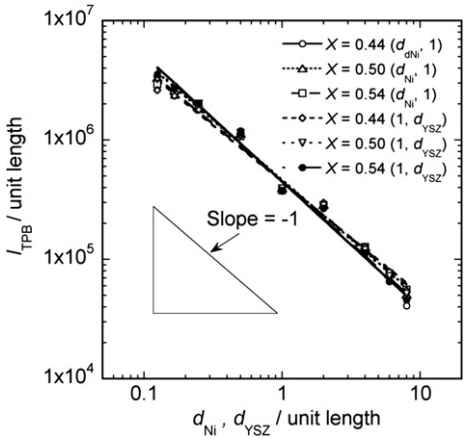

Fig. 5. l_{TPB} as a function of nickel-site size d_{Ni} and YSZ-site size d_{YSZ}. The fitted lines correspond to the power function regression curves represented by Eq. (2).

Table 3
The coefficient and the power exponent in Eq. (2) obtained by the regression analysis between the triple phase boundary length and the site sizes.

X	Valuable (unit length)	Coefficient A (unit length^{1-n})	Power exponent, n
0.44	d_{Ni}	4.32×10^5	−1.06
	d_{YSZ}	4.32×10^5	−0.94
0.50	d_{Ni}	4.54×10^5	−1.00
	d_{YSZ}	4.54×10^5	−1.00
0.54	d_{Ni}	4.42×10^5	−0.96
	d_{YSZ}	4.42×10^5	−1.04

on the porosity. Substituting Eqs. (4) and (5) into Eq. (1), the current density is expressed as

$$j = \frac{\dfrac{k_1 k_4}{d_{Ni} d_{YSZ}} \left\{ \exp\left(\dfrac{\alpha_a z F \eta}{RT}\right) - \exp\left(-\dfrac{\alpha_c z F \eta}{RT}\right) \right\}}{1 + \dfrac{k_1}{k_2} \exp\left(\dfrac{\alpha_a z F \eta}{RT}\right) + \dfrac{k_1}{k_3} \exp\left(-\dfrac{\alpha_c z F \eta}{RT}\right)}. \tag{6}$$

Moreover, by substituting electrochemical parameters from the experimental results in Table 1 (for the case of the largest particle–size combination (d_{Ni}, d_{YSZ}) = (200, 0.35) with $X = 0.44$ at 1273 K) into Eq. (6), the current–potential curve for the Ni/YSZ cermet anode as a function of particle sizes is summarized as follows:

$$j = \frac{\dfrac{1.53 \times 10^4}{d_{Ni} d_{YSZ}} \left\{ \exp\left(\dfrac{0.89 F \eta}{RT}\right) - \exp\left(-\dfrac{1.15 F \eta}{RT}\right) \right\}}{1 + 1.80 \times 10^{-2} \exp\left(\dfrac{0.89 F \eta}{RT}\right) - 1.14 \times 10^{-2} \exp\left(-\dfrac{1.15 F \eta}{RT}\right)} \tag{7}$$

By substituting the experimental conditions, $j = 2.00 \times 10^3$ A m^{-2} and $T = 1273$ K into Eq. (7), following relation is derived.

$$\frac{1.53 \times 10^4}{d_{Ni} d_{YSZ}} \{\exp(8.15\eta) - \exp(-10.5\eta)\} - 2.00 \times 10^3 \left\{1 + 1.80 \times 10^{-2} \exp(8.15\eta) - 1.14 \times 10^{-2} \exp(-10.5\eta)\right\} = 0 \tag{8}$$

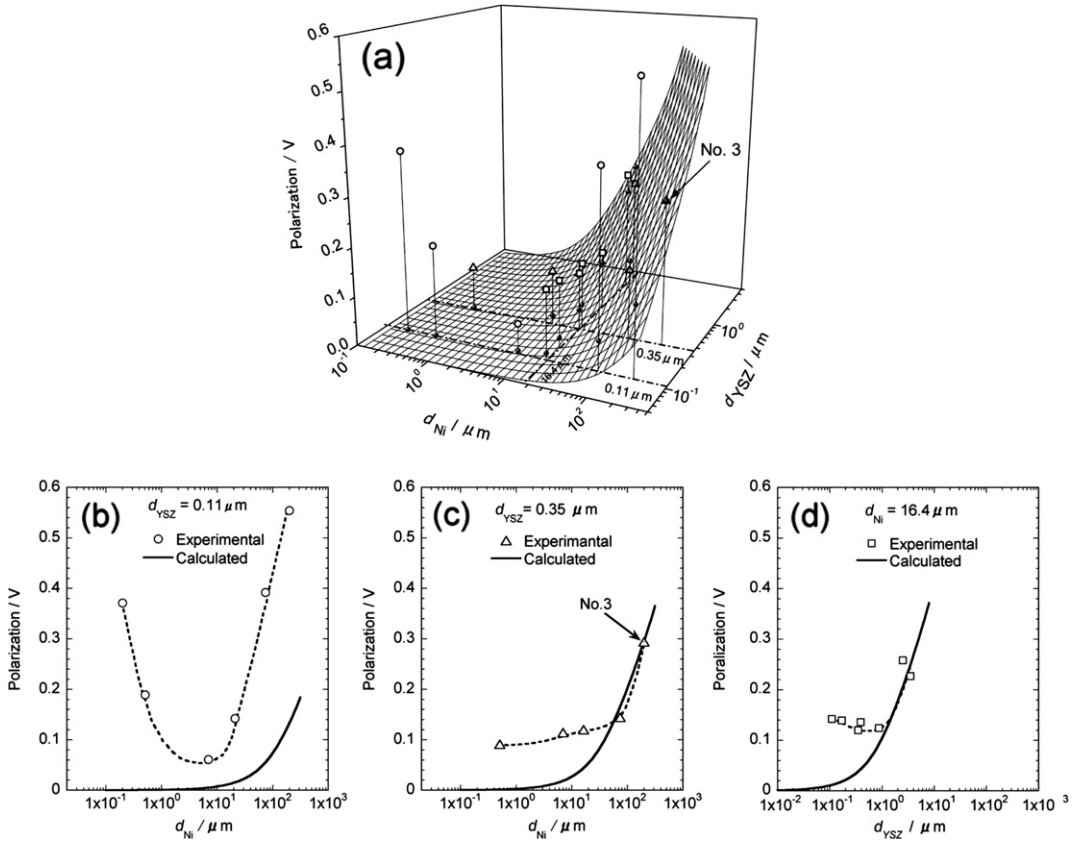

Fig. 6. (a) Anodic polarization of Ni/YSZ cermet anodes at a current density of 2.00×10^3 A m^{-2} as a function of particle diameter. Open symbols correspond to experimental values and the mesh surface represents the analytical solution of Eq. (8). Cross-sectional views of the mesh surface in (a) and the corresponding experimental values for cross-sectional planes of (b) $d_{YSZ} = 0.11$ μm, (c) $d_{YSZ} = 0.35$ μm, and (d) $d_{Ni} = 16.4$ μm, respectively.

By solving the above equation for η, the polarization at a current density of 2.00×10^3 A m^{-2} is obtained at given particle sizes. Fig. 6(a) shows a three-dimensional graph of the polarization as a function of d_{Ni} and d_{YSZ} calculated from the present model by the bi-section method [25], together with experimental data. The cross-sectional views by planes of (b) $d_{YSZ} = 0.11$ μm, (c) $d_{YSZ} = 0.35$ μm, and (d) $d_{Ni} = 16.4$ μm are also shown for clarity.

It is confirmed that the calculated polarization increases monotonically with increasing both d_{Ni} and d_{YSZ}. Therefore, the polarization becomes small when the values of d_{Ni} and d_{YSZ} are small. In contrast, the experimental polarization is a positively convex function of d_{YSZ} and d_{Ni}. For the case of $d_{YSZ} = 0.35$ μm, the experimental values agree well with the calculated ones at $d_{Ni} \geq 74$ μm except for $d_{Ni} \leq 7.0$ μm. For the case of $d_{Ni} = 16.4$ μm, the experimental values are in good agreement with the calculated ones with $d_{YSZ} \geq 0.87$ μm except for $d_{YSZ} \leq 0.39$ μm. On the other hand, the calculated polarization values are inconsistent with the experimental ones at $d_{YSZ} = 0.11$ μm. This inapplicability can be explained by secondary particle formation [19]. Therefore, Eq. (7) can reproduce the relationship between the polarization and particle sizes of the starting powders well in the range of large particle size. Consequently, inasmuch as secondary particle formation does not occur, crushing after pre-calcination is effective to reduce the anodic polarization [9].

5. Conclusions

By measuring the steady-state anodic polarization and performing Monte Carlo simulation, the particle size dependence on the polarization of Ni/YSZ cermet anodes for SOFCs is investigated. In the larger particle size range, the polarization is proved to be reduced by decreasing both of the nickel-particle size, d_{Ni}, and the YSZ-particle size, d_{YSZ}. In contrast, in the smaller particle size range, the polarization increases by decreasing the particle sizes. The TPB length in the model system is estimated using a Monte Carlo simulation on the basis of the simple cubic lattice model. It is confirmed that the TPB length is positively concave with respect to the nickel-volume fraction, X, for all site size combinations (d_{Ni}, d_{YSZ}). The TPB length for (1, 1) reaches a maximum at $X = 0.50$, and the maximal value of the TPB length decreases with increasing either d_{Ni} or d_{YSZ}. Moreover, the X value to give the maximal TPB length becomes larger and smaller than 0.50 when $d_{Ni}/d_{YSZ} > 1$ and $d_{Ni}/d_{YSZ} < 1$, respectively. The calculation results agree well with the experimental results obtained using FIB-SEM under same conditions.

On the basis of the experimental and calculation results obtained, the steady-state current–potential curve as a function of particle sizes is estimated for the nickel-volume fraction of 0.44 and at 1273 K. Moreover, estimated polarizations at a current density of 2.00×10^3 A m^{-2} in the larger particle size range are compared with the experimental results. The present study propose a possible model to estimate the electrochemical polarization of Ni/YSZ cermet anode as a function of the particle sizes of the starting powders in the range of large particle sizes, providing a useful guideline to control the fabrication process of SOFC anodes.

Appendix A. Derivation of the steady-state polarization curve

Here, an analytical equation for the polarization of the Ni/YSZ cermet anode as a function of the nickel-particle size, d_{Ni}, and the YSZ-particle size, d_{YSZ}, is derived as follows. The steady-state polarization curve of the electrode reaction at TPB of the Ni/YSZ cermet anode/YSZ electrolyte is described as the general Butler–Volmer equation, if one takes the concentrations of the oxidant and those of the reductant into account as follows:

$$j = j_0 \left\{ \frac{C_R^*}{C_R^b} \exp\left(\frac{\alpha_a z F \eta}{RT}\right) - \frac{C_O^*}{C_O^b} \exp\left(-\frac{\alpha_c z F \eta}{RT}\right) \right\}, \tag{A.1}$$

where C_R and C_O are the concentration of the reductant and the oxidant (mol m^{-3}) and subscripts * and b represent TPB and bulk, respectively. In addition, j and other parameters and constants are the same as defined in the main text.

Eq. (A.1) is rewritten as a function consisting of limiting current densities on behalf of the concentration of the reactant, because the limiting current densities are independent of the current density, whereas C_R^* and C_O^* depend on the current density. The anodic current density $j_{a,d}$ (A m^{-2}) and the cathodic current density $j_{c,d}$ (A m^{-2}) are derived from Fick's first law and Faraday's law of electrolysis by the following equations under the assumption of the Nernst diffusion layers, in which mass transfer occurs by linear diffusion as follows [26],

$$j_{a,d} = zFD_R \frac{C_R^b - C_R^*}{\delta_{N,a}}, \tag{A.2}$$

and,

$$j_{c,d} = zFD_O \frac{C_O^b - C_O^*}{\delta_{N,c}}, \tag{A.3}$$

where D_R and D_O are the diffusion coefficient of the reductant and the oxidant (m^2 s^{-1}) and $\delta_{N,a}$ and $\delta_{N,c}$ are the thickness of the diffusion layer of the reductant and the oxidant (m), respectively. When $C_R^* = 0$ and $C_O^* = 0$, Eqs. (A.2) and (A.3) give the limiting anodic current density $j_{a,l}$ (A m^{-2}) and the limiting cathodic current density $j_{c,l}$ (A m^{-2}), respectively, as

$$j_{a,l} = zFD_R \frac{C_R^b}{\delta_{N,a}} \tag{A.4}$$

and

$$j_{c,l} = -zFD_O \frac{C_O^b}{\delta_{N,c}}. \tag{A.5}$$

By combining Eqs. (A.2), (A.3), (A.4) and (A.5), we obtain

$$\frac{C_R^*}{C_R^b} = 1 - \frac{j_{a,d}}{j_{a,l}}, \tag{A.6}$$

and,

$$\frac{C_O^*}{C_O^b} = 1 + \frac{j_{c,d}}{j_{c,l}}. \tag{A.7}$$

Substituting Eqs. (A.6) and (A.7) into Eq. (A.1), the following equation is obtained.

$$j = j_0 \left\{ \left(1 - \frac{j_{a,d}}{j_{a,l}}\right) \exp\left(\frac{\alpha_a z F \eta}{RT}\right) - \left(1 + \frac{j_{c,d}}{j_{c,l}}\right) \exp\left(-\frac{\alpha_c z F \eta}{RT}\right) \right\} \tag{A.8}$$

The flux of the reductant to TPB, that of the oxidant from the TPB and the charge-transfer reaction rate should be equal for continuity constrain. Then,

$$j = j_{a,d} = j_{c,d}. \tag{A.9}$$

Therefore, Eq. (A.8) can be rewritten as

$$j = j_0\left\{\left(1-\frac{j}{j_{a,l}}\right)\exp\left(\frac{\alpha_a zF\eta}{RT}\right)-\left(1+\frac{j}{j_{c,l}}\right)\exp\left(-\frac{\alpha_c zF\eta}{RT}\right)\right\}. \tag{A.10}$$

By reformatting Eq. (A.10) as a function of j, the expression for the steady-state polarization is derived as follows.

$$j = \frac{j_0\left\{\exp\left(\frac{\alpha_a zF\eta}{RT}\right)-\exp\left(-\frac{\alpha_c zF\eta}{RT}\right)\right\}}{1+\frac{j_0}{j_{a,l}}\exp\left(\frac{\alpha_a zF\eta}{RT}\right)+\frac{j_0}{j_{c,l}}\exp\left(-\frac{\alpha_c zF\eta}{RT}\right)} \tag{A.11}$$

References

[1] E. Baur, H. Preis, Z. Elektrochem. 43 (1937) 727–732.
[2] H.H. Möbius, J. Solid State Electrochem. 1 (1997) 2–16.
[3] A. Atkinson, S. Barnett, R.J. Gorte, J.T.S. Irvine, A.J. McEvoy, M. Mogensen, S.C. Singhal, J. Vohs, Nat. Mater. 3 (2004) 17–27.
[4] H.S. Spacil, US-P 3, 503, 809, filed 30, 10, 1964 (1970).
[5] S. Murakami, Y. Akiyama, N. Ishida, Y. Miyake, M. Nishioka, Y. Itoh, T. Saito, N. Furukawa, Denki Kagaku 59 (1991) 320–324.
[6] T. Saito, Y. Akiyama, N. Ishida, T. Yasuo, S. Taniguchi, S. Murakami, N. Furukawa, Denki Kagaku 61 (1993) 228–233.
[7] H. Koide, Y. Someya, T. Yoshida, T. Maruyama, Solid State Ionics 132 (2000) 253–260.
[8] F.P.F. van Berkel, F.H. van Heuveln, J.P.P. Hujismans, Solid State Ionics 72 (1994) 240–247.
[9] T. Kawada, N. Sakai, H. Yokokawa, M. Dokiya, M. Mori, T. Iwata, J. Electrochem. Soc. 137 (1990) 3042–3047.
[10] S. Primidahl, B.F. Sørensen, M. Mogensen, J. Am. Ceram. Soc. 83 (2000) 489–494.
[11] J. Mizusaki, H. Tagawa, T. Saito, T. Yamamura, K. Kamitani, K. Hirano, S. Ehara, T. Takagi, T. Hikita, M. Ippommatsu, S. Nakagawa, K. Hashimoto, Solid State Ionics 70/71 (1994) 52–58.
[12] J. Mizusaki, H. Tagawa, T. Saito, K. Kamitani, T. Yamamura, K. Hirano, S. Ehara, T. Takagi, T. Hikita, M. Ippommatsu, S. Nakagawa, K. Hashimoto, J. Electrochem. Soc. 141 (1994) 2129–2134.
[13] A. Bieberle, L.P. Meier, L.J. Gauckler, J. Electrochem. Soc. 148 (2001) A646–A656.
[14] A. Bieberle, L.J. Gauckler, Solid State Ionics 146 (2002) 23–41.
[15] J.R. Wilson, W. Kobsiriphat, R. Mendoza, H.-Y. Chen, J.M. Hiller, D.J. Miller, K. Thornton, P.W. Voorhees, S.B. Adler, S.A. Barnett, Nat. Mater. 5 (2006) 541–544.
[16] H. Iwai, N. Shikazono, T. Matsui, H. Teshima, M. Kishimoto, R. Kishida, D. Hayashi, K. Matsuzaki, D. Kanno, M. Saito, H. Muroyama, K. Eguchi, N. Kasagi, H. Yoshida, J. Power Sources 195 (2010) 955–961.
[17] N. Shikazano, D. Kanno, K. Matsuzaki, H. Teshima, S. Sumino, N. Kasagi, J. Electrochem. Soc. 157 (2010) B665–B672.
[18] N. Vivet, S. Chupin, E. Estrade, A. Richard, S. Bonnamy, D. Rochais, E. Bruneton, J. Power Sources 196 (2011) 9989–9997.
[19] T. Kawashima, Y. Matsuzaki, J. Ceram. Soc. Jpn. 104 (1996) 317–321.
[20] W.H. Press, S.A. Teukolsky, W.T. Vetterling, B.P. Flannery, Numerical Recipes in C the Art of Scientific Computing, second ed., Cambridge University Press, Cambridge, 1992, pp. 683–688.
[21] R.E. Williford, L.A. Chick, G.D. Maupin, S.P. Simner, J.W. Stevenson, J. Electrochem. Soc. 150 (2003) A1067–A1072.
[22] J. Hoshen, R. Kopelman, Phys. Rev. B 14 (1976) 3438–3445.
[23] V.M. Janardhanan, V. Heuveline, O. Deutschmann, J. Power Sources 178 (2008) 368–372.
[24] S. Sakamoto, H. Taira, H. Takagi, Denki Kagaku 64 (1996) 609–613.
[25] W.H. Press, S.A. Teukolsky, W.T. Vetterling, B.P. Flannery, Numerical Recipes in C the Art of Scientific Computing, second ed., Cambridge University Press, Cambridge, 1992, pp. 353–354.
[26] S. Haruyama, Hyomen Gijyutsusya no-tame-no Denki Kagaku Ver. 2, Maruzen, Tokyo, 2005, pp. 87–108.